Research article

Markus Rösch*, Mattias Beck, Martin J. Süess, Dominic Bachmann, Karl Unterrainer, Jérôme Faist and Giacomo Scalari*

Heterogeneous terahertz quantum cascade lasers exceeding 1.9 THz spectral bandwidth and featuring dual comb operation

https://doi.org/10.1515/nanoph-2017-0024
Received February 7, 2017; revised May 8, 2017; accepted May 10, 2017

Abstract: We report on a heterogeneous active region design for terahertz quantum cascade laser based frequency combs. Dynamic range, spectral bandwidth and output power have been significantly improved with respect to previous designs. When individually operating the lasers, narrow and stable intermode beatnote indicate frequency comb operation up to a spectral bandwidth of 1.1 THz, while in a dispersion-dominated regime a bandwidth up to 1.94 THz at a center frequency of 3 THz can be reached. A self-detected dual-comb setup has been used to verify the frequency comb nature of the lasers.

Keywords: terahertz; frequency comb; quantum cascade laser.

The quantum cascade laser (QCL) is an established coherent source for wavelengths between 3 μm and 300 μm [1–4]. Especially in the so-called terahertz (THz) frequency range (roughly 1–10 THz or 30–300 μm) QCLs are a compact direct source providing high power up to the watt level [2, 5]. Due to its inherent properties, QCLs can be designed to cover a very broad spectral range with a single device [6–8], making them an attractive source for broadband spectroscopy. Frequency combs (FCs) have recently been reported as a tool for spectroscopic applications with QCLs [8–10]. So-called dual-comb spectroscopy is particularly interesting at both midinfrared and THz frequencies [11–18]. To achieve FC operation using a THz QCL, the dispersion of the laser has to be engineered to be close to 0 for the frequency range of operation [8, 10]. Two different approaches have been reported to achieve low and flat dispersion in THz QCLs. The first one introduces negative dispersion to compensate for the positive intrinsic dispersion of narrow waveguides with a double-chirped mirror [10]. The alternative approach uses wider waveguides in combination with a broad gain medium which provides a low and flat intrinsic dispersion at the center of the gain curve [8, 17, 19]. The spectral range of the FC is in that case directly related to the gain curve [19]. A wider gain curve will allow FC operation as long as the gain curve remains flat [8, 19]. However, it needs to be noted that a FC operation on the full laser bandwidth will only be possible by artificially introducing additional dispersion, i.e. by a Gires-Tournois interferometer [20, 21], or a double-chirped mirror [10, 22].

THz QCL based FCs have the advantage overexisting THz FCs based on photoconductive emitters to provide a higher brightness in more compact form and higher efficiencies [14, 15]. However, it can be envisioned that the latest development on highly efficient broadband photoconductive emitters using fiber laser as a pump source will allow in the future also compact and efficient FCs based on that technology [23, 24].

In this work, we present a THz QCL active region design based on a heterogeneous cascade structure that expands both the total laser bandwidth and the FC bandwidth. This shows that indeed by gain engineering the dispersion can be further compensated and larger FC bandwidths can be achieved. In addition, also, the dynamic range as well as the output power are increased. An experiment similar to the one reported in Ref. [17] has been used to verify the FC operation in a dual-comb configuration.

The laser active region we present here is based on the design reported in Ref. [8], which has been further developed. It fully exploits the capability of QCLs to integrate

***Corresponding authors: Markus Rösch and Giacomo Scalari,** ETH Zurich, Institute of Quantum Electronics, Auguste-Piccard-Hof 1, 8093 Zurich, Switzerland, e-mail: mroesch@phys.ethz.ch (M. Rösch); scalari@phys.ethz.ch (G. Scalari)
Mattias Beck, Martin J. Süess and Jérôme Faist: ETH Zurich, Institute of Quantum Electronics, Auguste-Piccard-Hof 1, 8093 Zurich, Switzerland
Dominic Bachmann and Karl Unterrainer: TU Wien, Photonics Institute and Center for Micro- and Nanostructures, Gußhausstraße 27-29, 1040 Vienna, Austria

different active region designs within one laser cavity [6]. The used building block is a design which by itself is already intrinsically broadband, a four-quantum-well design reported originally in Ref. [25]. This active region was then adapted to have four designs with slightly different central frequencies. The four designs have central frequencies of 2.3, 2.6, 2.9, and 3.4 THz. While the three lower frequency designs are identical with those from Ref. [8], the design at 3.4 THz has been added to increase the bandwidth towards higher frequencies. The number of periods per design has also been rearranged in order to provide a flat gain resulting in a similar threshold for all the active regions and more dynamic range. Additionally, the doping level has been increased to 2.2×10^{16} cm^{-3}. The exact layer sequences are reported in the Appendix.

Lasers were fabricated into metal-metal waveguides for best performance [8, 26, 27]. Both wet-etching and dry-etching techniques have been used to define the laser ridges. Wet-etched lasers typically provide the best results in pulsed operation, while dry-etched lasers can be fabricated into narrower ridges and therefore have reduced Joule heating for the same cavity length which favors continuous wave (CW) operation [27].

Figure 1A shows the light-current and current-voltage (LIV) characteristics of a 2 mm×150 µm wet-etched laser in pulsed operation. The laser shows up to 10 mW of output power at 10 K. Lasing occurs up to a temperature of 100 K. For comparison, the LIV of a laser with the same dimensions of the design reported in Ref. [8] is shown along in Figure 1A. We observe roughly 40% more power

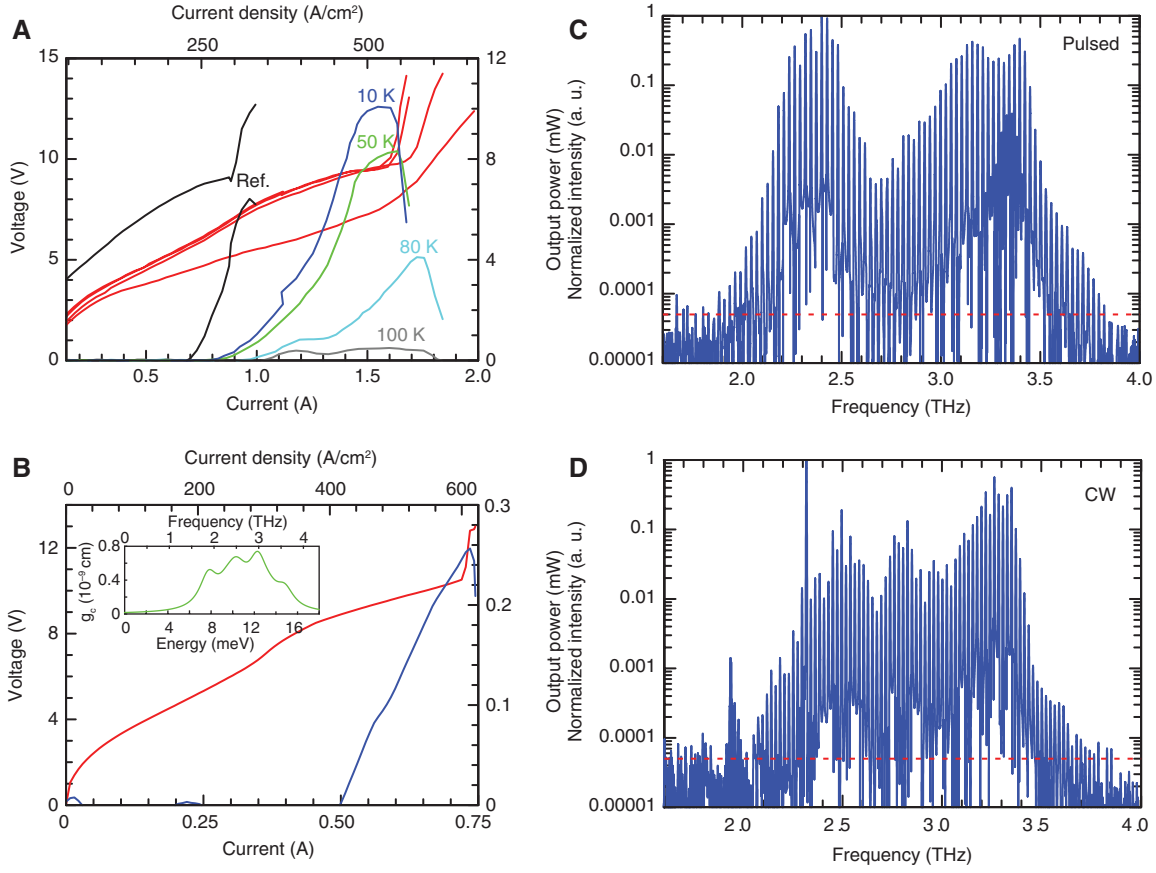

Figure 1: Laser characteristics: (A) Light-current and current-voltage characteristics for a 2 mm×150 µm wet-etched laser in pulsed operation at different temperatures. To emphasize the improvements, a reference measurement of a laser with the same dimensions (black curves) based on the design reported in Ref. [8] is shown. The measurements were performed in pulsed operation with 10% duty cycle (5% for the 100 K measurement). The optical power was measured with a calibrated powermeter (TK instruments). (B) Light-current and current-voltage characteristics for a 2 mm×60 µm dry-etched laser in CW operation at 20 K. The power was measured with a calibrated powermeter (Ophir:3A-P-THz). The inset shows the calculated gain cross-section g_c of the reported laser design. (C) Optical spectrum of a 1.5 mm×150 µm wet-etched laser in pulsed operation (20% duty cycle) at 20 K. (D) Optical spectrum of a 1.8 mm×60 µm dry-etched laser in CW operation at 21 K. The spectra in (C) and (D) were measured using a commercial vacuum FTIR (Bruker v80) using the internal room temperature deuterated triglycine sulfate detector. The red dashed lines indicate roughly the noise floor of the measurements.

on the reported design. Additionally, the dynamic range of the laser is significantly improved. While for the reference laser of Ref. [8] a dynamic range (J_{max}/J_{th}) of 1.4 was measured, the reported design shows a dynamic range of 2. We attribute the improvement of the dynamic range to the careful rearrangement of the active region, while the improvement in output power is due to a combination of the higher doping level as well as the increased number of cascades in the active region. The higher doping level also causes a slightly higher threshold current.

Dry-etched lasers were used to test the CW performance of the reported active region. Figure 1B shows the LIV characteristics for a 2 mm × 60 µm dry-etched laser in CW operation at 20 K. An optical power of 0.26 mW was measured using a calibrated powermeter (Ophir:3A-P-THz). Operation up to a temperature of 30 K is achieved in CW operation.

Since the reported laser features an additional active region design with a central frequency at 3.4 THz, the optical spectrum has an upper limit at almost 4 THz as can be seen in Figure 1C. The spectra were measured using a commercial under-vacuum Fourier-transform infrared spectrometer (FTIR). In total, the lasing spectrum spans over 1.94 THz from 1.88 THz to 3.82 THz covering more than a full octave in frequency. The spectrum is in good agreement with the calculated gain cross-section (inset of Figure 1B using the same model as in Ref. [8]. A similar performance can also be observed in CW for dry-etched lasers. As shown in Figure 1D the lowest frequencies below 2 THz do not reach lasing threshold in dry-etched lasers. Most likely, this is due to increased waveguide losses of the narrow dry-etched waveguide (60 µm) at low frequencies in combination with the large Joule heating which also prevents the laser from reaching high operation temperatures in CW operation. Zoomed versions of the spectra reported here are shown in Supplementary Figure 1.

It has recently been shown that THz QCLs with a broad spectral gain have sufficiently low and flat dispersion to operate as FC for a limited part of the laser's dynamic range [8, 17]. Similar behavior can be expected from the reported laser design as it covers an even larger spectral part. The key indicator of comb operation in QCLs is the radio frequency (RF) beatnote signal at the roundtrip frequency of the laser cavity (f_{rep}). A single narrow beatnote at f_{rep} is indicating comb operation, while a broad beatnote is characteristic for a lasing regime where the group velocity dispersion is large enough to prevent the four-wave mixing to lock the lasing modes [8–10, 17, 28]. Throughout the entire dynamic range of the laser the RF beatnote around the roundtrip frequency of the laser is recorded using a bias tee on the bias line and a RF spectrum analyzer (Rohde & Schwarz FSU50). The corresponding beatnote map for a 2 mm × 60 µm dry-etched laser is shown in Figure 2A. The performance is similar to the one reported in Ref. [8]. For lower currents a single narrow beatnote is observed, while for higher currents dispersion sets in preventing comb operation and resulting in a broad beatnote. Figure 2B shows the optical spectrum at the highest bias point with a narrow beatnote (562 mA). A spectral bandwidth of 1.1 THz is recorded at a central frequency of 3.1

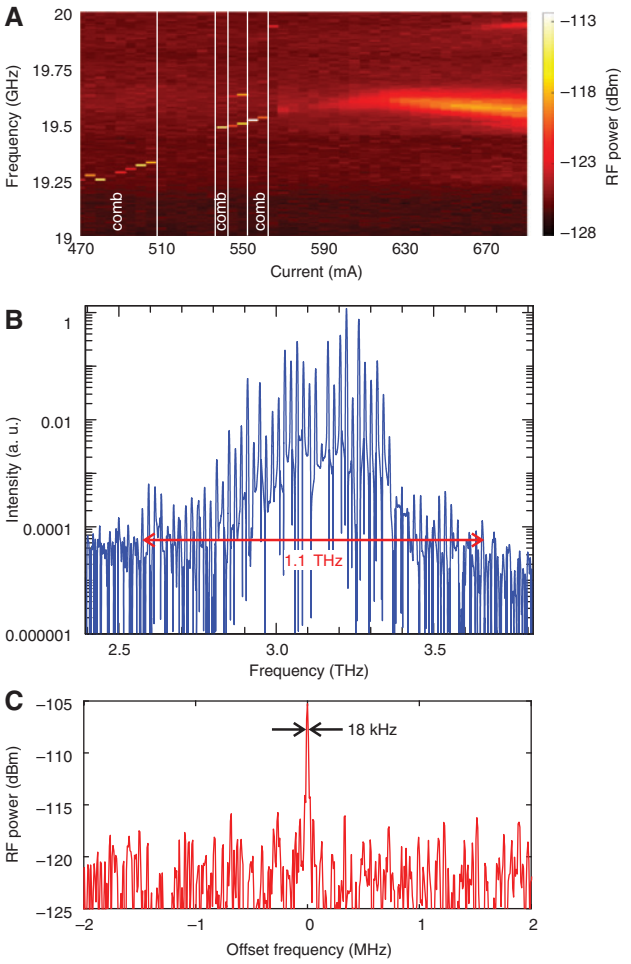

Figure 2: Frequency comb performance: (A) Intermode beatnote of a 2 mm × 60 µm dry-etched laser as a function of the driving current. The temperature is fixed to 20 K. The beatnote signal is extracted from the bias line with a bias-tee and is recorded with an RF spectrum analyzer (Rohde & Schwarz FSU50; RBW: 10 kHz, video bandwidth (VBW): 100 kHz, sweep time (SWT): 10 s). (B) Optical spectrum for the same laser at 562 mA at 16 K. For this current the laser is in a FC regime providing a bandwidth of 1.1 THz. (C) Intermode beatnote of the same laser under the same driving conditions as in (B) recorded with an RF spectrum analyzer (RBW: 10 kHz, VBW: 100 kHz, SWT: 20 ms). The linewidth is limited by the RBW of the spectrum analyzer.

THz. To our knowledge this is the broadest THz QCL FC so far reported (see also Supplementary Figure 2). The intermode beatnote under these driving conditions is reported in Figure 2C showing a linewidth limited by the resolution bandwidth (RBW) of the spectrum analyzer. A signal-to-noise ratio of approximately 15 dB is achieved.

A narrow beatnote at the roundtrip frequency of the laser is a necessary but not a sufficient condition to prove FC operation [8, 10, 17]. Beatnote spectroscopy or shifted wave interference Fourier transform spectroscopy experiments that prove the comb operation are difficult to perform at THz frequencies due to the lack of fast and sensitive enough detectors [9, 10]. Another approach to prove the comb behavior of a QCL comb is to perform a dual-comb experiment [16, 17]. Such an experiment will directly reveal the comb characteristics of the two lasers used for the experiment. For THz QCL combs a self-detection dual-comb configuration allows a straight-forward implementation of that experiment without the need of an external detector [17].

Two lasers mounted on the same chip parallel to each other have been used to perform this experiment in analogy to Ref. [17]. The two lasers have the dimensions of 2 mm × 60 µm and were driven in CW operation at a temperature of 26 K. The lasers are separated 450 µm, and hence a similar coupling efficiency as reported in Ref. [17] can be expected. A dual-comb regime was identified in a first step by the presence of two narrow beatnotes at the roundtrip frequencies of the two lasers (see inset of Figure 3). For the same driving conditions the optical spectrum of the two lasers was recorded with an FTIR. The corresponding optical spectrum in Figure 3 (blue curve) shows a single set of equally spaced modes. This hints that the offset between the two sets of comb modes is lower than the resolution of the FTIR (2.25 GHz). Additionally, this will not allow to make any prediction in the mode intensities of the multiheterodyne spectrum. Indeed, the multiheterodyne spectrum is located between 0.5 and 1.5 GHz (red curve in Figure 3). Nine modes can be identified with a mode spacing of 106 MHz in good agreement with the spacing of the intermode beatnotes as well as the recorded optical spectrum. Similar to the results presented in Ref. [17], the intermode beatnote linewidth remains similar as in single FC operation, while for the modes of the multiheterodyne signal a linewidth of ~3.2 MHz is measured.

The multiheterodyne spectrum corresponds to an optical bandwidth of 175 GHz. This is significantly less than the reported bandwidth for a single device in Figure 2B. This can be attributed to the large Joule heating when two lasers are driven in CW operation at the same time on the same cryostat. For the same reason it was

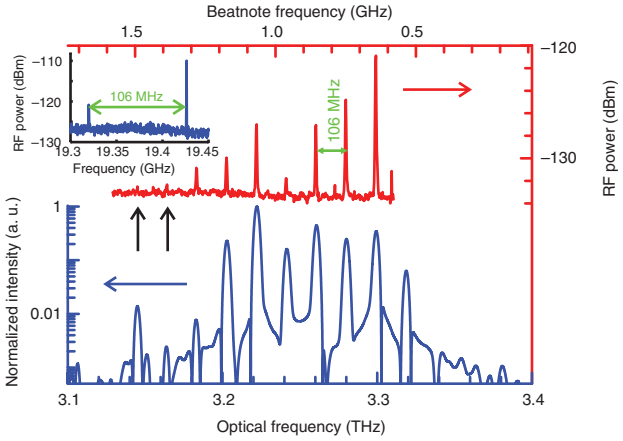

Figure 3: Dual-comb experiment: FTIR (Bruker 80v) measurement of two lasers operating as FCs (blue curve). The two lasers are both 2 mm × 60 µm. Laser 1 is driven at 595 mA and laser 2 at 550 mA. The temperature is fixed to 26 K. Only a single set of modes is observed as the offset between the two sets of laser modes is below the resolution limit of the FTIR (2.25 GHz). The red curve is the corresponding multiheterodyne spectrum recorded with an RF spectrum analyzer (Rohde & Schwarz FSU50; RBW: 2 kHz, VBW: 20 kHz, SWT: 250 s). The signal was extracted with a bias-tee from the bias line of one of the two lasers. The two black arrows indicate the positions of the two weakest modes of the multiheterodyne spectrum. The RF signal is truncated below 0.6 GHz due to strong pickup noise in the experimental setup. The inset shows the two intermode beatnotes of the two lasers (RBW: 10 kHz, VBW: 100 kHz, SWT: 2 s).

not possible to cool down the two lasers to temperatures below 25 K while for a single laser operation temperatures down to 15 K can be achieved with the same helium-flow cryostat. Therefore, the lasers had to be operated close to their maximal operation temperature, which significantly decreases the spectral bandwidth. However, the measurements in Figure 2 clearly show that the reported laser is indeed working as a FC supporting the FC identification through the beatnote measurements in Figure 2A. Experimentally, a narrow intermode beatnote has always been identified with FC operation in unmodulated QCLs [9, 10, 16, 17, 21]. This identification is also supported by theoretical models [28].

In summary, we presented a heterogeneous cascade active region design for THz QCLs based on four active region designs. The lasers show a spectral bandwidth of almost 2 THz at a central frequency of 3 THz. A peak output power of 10 mW in pulsed operation was achieved with a dynamic range of $J_{max}/J_{th} = 2$. A spectral bandwidth of 1.1 THz was measured while observing a narrow intermode beatnote indicating FC operation. To confirm FC operation, a self-detected dual-comb experiment was performed. We could confirm the FC operation on a bandwidth of 175 GHz. The bandwidth in this experiment was

temperature limited, and therefore only a limited part of the effective FC spectrum could be probed. To conclude, we could show that with careful designing and balancing of the involved active region designs, the spectra of THz QCLs can be further pushed to bandwidths exceeding an octave in frequency. Considerable efforts needed to be done to achieve such a well-balanced gain while keeping the Joule heating resulting from the laser bias low enough to allow CW operation. An unbalanced gain will result in reduced spectral performance and can also result in electrical instabilities of the laser [7]. Ideally, further improvements will lead to lasers where an octave bandwidth within a 20 dB power range can be reached. Such power constraints will be necessary for a potential f-to-2f stabilization in QCL FCs [29, 30]. FC operation over a full octave should be possible in the future using an appropriate dispersion compensation such as double-chirped mirrors [10, 31].

The ability to temperature and current tune QCLs over a full free spectral range for long laser cavites is also attractive for QCL-based FCs [32]. It will allow to have a spectroscopy tool that provides continuous frequency coverage combined with high frequency accuracy.

Acknowledgments: The presented work was funded by the EU research project TERACOMB (Call identifier FP7-ICT-2011-C, Project No. 296500), and the Swiss National Science Foundation (SNF) grant 200020 165639. The funding is gratefully acknowledged. The authors acknowledge the joint cleanroom facility FIRST at ETH Zurich and the Center for Micro- and Nanostructures (ZMNS) at TU Wien for sample processing.

Appendix

Quantum cascade layer sequence and details

Sample EV2172 has been grown by molecular beam epitaxy on a semi-insulating GaAs substrate in the GaAs/AlGaAs material systems. The layer sequence for the 3.4 THz active region (64 repetitions) is, starting from the injection barrier, as follows: **5.5**/10.7/**1.4**/10.1/**3.8**/9.2/**4.2**/18.0. The figures in boldface represent the $Al_{0.15}Ga_{0.85}As$ barrier, and the 18.0 nm GaAs quantum well is homogeneously Si doped 2.2×10^{16} cm^{-3}. The layer sequence for the 2.9 THz active region (34 repetitions) is, starting from the injection barrier, as follows: **5.5**/11.0/**1.8**/11.5/**3.8**/9.4/**4.2**/18.4. The 18.4 nm GaAs quantum well is homogeneously Si doped 2.2×10^{16} cm^{-3}. The layer sequence for the 2.6 THz active region (39 repetitions) is, starting from the injection barrier: **5.5**/11.3/**1.8**/11.3/**3.8**/9.4/**4.2**/18.4. The 18.4 nm GaAs quantum well is homogeneously Si doped 2.2×10^{16} cm^{-3}. The layer sequence for the 2.3 THz active region (73 repetitions) is, starting from the injection barrier as follows: **5.5**/12.0/**1.8**/10.5/**3.8**/9.4/**4.2**/18.4. The 18.4 nm GaAs quantum well is homogeneously Si doped 2.2×10^{16} cm^{-3}. The three lower frequency layer sequences are identical with those reported in references [7, 8]. Modifications have been done on the number of repetitions and the Si doping level.

References

[1] Faist J, Capasso F, Sivco DL, Sirtori C, Hutchinson AL, Cho AY. Quantum cascade laser. Science 1994;264:553–6.
[2] Williams BS. Terahertz quantum-cascade lasers. Nat Photonics 2007;1:517–25.
[3] Scalari G, Walther C, Fischer M, et al. THz and sub-THz quantum cascade lasers. Laser Photon Rev 2009;3:45–66.
[4] Revin DG, Cockburn JW, Steer MJ, et al. InGaAs/AlAsSb/InPInGaAs/AlAsSb/InP quantum cascade lasers operating at wavelengths close to 3 μm. Appl Phys Lett 2007;90:eid021108.
[5] Li L, Chen L, Zhu J, et al. Terahertz quantum cascade lasers with >1 W output powers. Electro Lett 2014;50:309–11.
[6] Gmachl C, Sivco DL, Colombelli R, Capasso F, Cho AY. Ultra-broadband semiconductor laser. Nature 2002;415:883–7.
[7] Turčinková D, Scalari G, Castellano F, Amanti MI, Beck M, Faist J. Ultra-broadband heterogeneous quantum cascade laser emitting from 2.2 to 3.2 THz. Appl Phys Lett 2011;99:191104.
[8] Rösch M, Scalari G, Beck M, Faist J. Octave-spanning semiconductor laser. Nat Photonics 2015;9:42–7.
[9] Hugi A, Villares G, Blaser S, Liu HC, Faist J. Mid-infrared frequency comb based on a quantum cascade laser. Nature 2012;492:229–33.
[10] Burghoff D, Kao TY, Han N, et al. Terahertz laser frequency combs. Nat Photonics 2014;8:462–7.
[11] Bernhardt B, Ozawa A, Jacquet P, et al. Cavity-enhanced dual-comb spectroscopy. Nat Photonics 2010;4:55–7.
[12] Baumann E, Giorgetta F, Swann W, Zolot A, Coddington I, Newbury N. Frequency-comb-based remote sensing of greenhouse gases over kilometer air paths. Phys Rev A 2011;84:062513.
[13] Zhang Z, Gardiner T, Reid DT. Mid-infrared dual-comb spectroscopy with an optical parametric oscillator. Opt Lett 2013;38:3148.
[14] Yasui T, Kabetani Y, Saneyoshi E, Yokoyama S, Araki T. Terahertz frequency comb by multifrequency-heterodyning photoconductive detection for high-accuracy, high-resolution terahertz spectroscopy. Appl Phys Lett 2006;88:eid241104.
[15] Finneran IA, Good JT, Holland DB, Carroll PB, Allodi MA, Blake GA. Decade-spanning high-precision terahertz frequency comb. Phys Rev Lett 2015;114:163902.
[16] Villares G, Hugi A, Blaser S, Faist J. Dual-comb spectroscopy based on quantum-cascade-laser frequency combs. Nat Commun 2014;5:5192.

[17] Rösch M, Scalari G, Villares G, Bosco L, Beck M, Faist J. On-chip, self-detected terahertz dual-comb source. Appl Phys Lett 2016;108:171104.
[18] Yang Y, Burghoff D, Hayton DJ, Gao JR, Reno JL, Hu Q. Terahertz multiheterodyne spectroscopy using laser frequency combs. Optica 2016;3:499.
[19] Bachmann D, Rösch M, Scalari G, et al. Dispersion in a broadband terahertz quantum cascade laser. Appl Phys Lett 2016;109:221107.
[20] Gires F, Tournois P. Prismless passively mode-locked femtosecond Cr:LiSGaF laser. CR Acad Sci 1964;258:6112.
[21] Villares G, Riedi S, Wolf J, et al. Dispersion engineering of quantum cascade laser frequency combs. Optica 2016;3:252.
[22] Szipöcs R, Spielmann C, Krausz F, Ferencz K. Chirped multilayer coatings for broadband dispersion control in femtosecond lasers. Opt Lett 1994;19:201.
[23] Hale PJ, Madeo J, Chin C, et al. 20 THz broadband generation using semi-insulating GaAs interdigitated photoconductive antennas. Opt Express 2014;22:26358.
[24] Yardimci NT, Yang SH, Berry CW, Jarrahi M. High-power terahertz generation using large-area plasmonic photoconductive emitters. IEEE Trans Terahertz Sci Technol 2015;5:223–9.
[25] Amanti MI, Scalari G, Terazzi R, et al. Bound-to-continuum terahertz quantum cascade laser with a single-quantum-well phonon extraction/injection stage. New J Phys 2009;11:125022.
[26] Williams BS, Kumar S, Callebaut H, Hu Q, Reno JL. Terahertz quantum-cascade laser at $\lambda \approx 100$-μm using metal waveguide for mode confinement. Appl Phys Lett 2003;83:2124–6.
[27] Bachmann D, Rösch M, Süess MJ, et al. Short pulse generation and mode control of broadband terahertz quantum cascade lasers. Optica 2016;3:1087.
[28] Khurgin JB, Dikmelik Y, Hugi A, Faist J. Coherent frequency combs produced by self frequency modulation in quantum cascade lasers. Appl Phys Lett 2014;104:eid081118.
[29] Telle H, Steinmeyer G, Dunlop A, Stenger J, Sutter D, Keller U. Carrier-envelope offset phase control: A novel concept for absolute optical frequency measurement and ultrashort pulse generation. Appl Phys B 1999;69:327–32.
[30] Jones DJ, Diddams SA, Ranka JK, et al. Carrier-envelope phase control of femtosecond mode-locked lasers and direct optical frequency synthesis. Science 2000;288:635–9.
[31] Xu C, Ban D. Design of chirped distributed Bragg reflector for octave-spanning frequency group velocity dispersion compensation in terahertz quantum cascade laser. Opt Express 2016;24:13500.
[32] Wienold M, Röben B, Schrottke L, Grahn HT. Evidence for frequency comb emission from a Fabry-Pérot terahertz quantum-cascade laser. Opt Express 2014;22:30410.

Supplemental Material: The online version of this article offers supplementary material (https://doi.org/10.1515/nanoph-2017-0024).